# A doxorubicin–platinum conjugate system: impacts on PI3K/AKT actuation and apoptosis in breast cancer cells†

Puja Patel,[*a] Devan Umapathy,[b] Selvambigai Manivannan,[c] Vinita Manimaran Nadar,[a] Rajiu Venkatesan,[d] Velanganni Antony Joseph Arokiyam,[b] Srinivasan Pappu[e] and Kumar Ponnuchamy [iD] [*a]

In recent years, the development of a nano-conjugate system for drug delivery applications has gained attention among researchers. Keeping this in mind, in this study, we developed a doxorubicin–platinum conjugate system that targeted breast cancer cell lines. To achieve this, we developed platinum nanoparticles using polyvinylpyrrolidone (PVP). High resolution-transmission electron microscopy (HR-TEM) revealed the occurrence of octopod-shaped platinum nanoparticles. Subsequently, doxorubicin (DOX) was conjugated on the surface of the as-prepared platinum octopods *via* an *in situ* stirring method. The physicochemical characterization of the doxorubicin–platinum conjugate system revealed that the PVP of PtNPs interacts with the $NH_2$ group of doxorubicin *via* electrostatic interaction/hydrogen bonding. Besides, the doxorubicin–platinum conjugate system exhibited a sustained drug release profile within the cancer cells. Furthermore, the evaluation of the *in vitro* anticancer efficacy of the doxorubicin–platinum conjugate system in breast cancer cells (MCF-7 and MDA-MB-231) unveiled the induction of apoptosis *via* intracellular ROS and DNA damage, rather than free DOX and PtNPs. Remarkably, we also perceived that the doxorubicin–platinum conjugate system was strong enough to down-regulate the PI3K/AKT signalling pathway. As a result, the tumour suppressor gene *PTEN* was activated, which led to the stimulation of a mitochondrion-based intrinsic apoptotic pathway and its downstream caspases, triggering cell death. Hence, our findings suggested that a biologically stable doxorubicin–platinum conjugate system could be an imperative therapeutic agent for anticancer therapy in the near future.

## 1. Introduction

In recent years, engineered nanoscale drug delivery systems offer specificity and pass multidrug resistance mechanisms, enabling a paradigm shift in cancer treatment.[1–3] In view of this, platinum-based drugs such as cisplatin, carboplatin, and oxaliplatin are used worldwide to treat patients.[4–6] However,

[a]Food Chemistry and Molecular Cancer Biology Lab, Department of Animal Health and Management, Alagappa University, Karaikudi 630 003, India. E-mail: kumarp@alagappauniversity.ac.in

[b]Molecular Oncology Lab, Department of Biochemistry, Bharathidasan University, Tiruchirappalli 620 024, Tamil Nadu, India

[c]Department of Biomedical Science, Centre for Membrane Interactions and Dynamics (CMIAD), The University of Sheffield, Western Bank, Sheffield, S10 2TN, UK

[d]MOE Key Laboratory of Macromolecular Synthesis and Functionalization, Department of Polymer Science and Engineering, Zhejiang University, Hangzhou 310027, China

[e]Phage Therapy and Molecular Biology Lab, Department of Animal Health and Management, Alagappa University, Karaikudi 630003, Tamil Nadu, India

† Electronic supplementary information (ESI) available. See DOI: 10.1039/d0ra06708c

adverse side effects and increased drug resistance results in lack of specificity towards cancer targets.[7] As a result, nano-formulations that involve inorganic platinum nanoparticles have not yet entered clinical studies so far.[8,9] Considering this fact, coating the surface of platinum nanomaterials with a biocompatible agent (*e.g.*, PVP), a synthetic polymer, could promote prolonged circulation within the biological system.[10] To date, several polymeric coated platinum-based nanoparticles are widely developed to study the electrochemical, catalytic properties, *etc.*[11–13] However, biological studies pertaining to polymeric platinum nanoparticles are limited.[14]

Doxorubicin is an anthracycline-ringed antibiotic that treats a wide range of diseases, including cancer. Owing to this fact, we considered doxorubicin to be a better choice for conjugation with platinum nanoparticles.[15,16] The conjugation of doxorubicin with organic and inorganic nanomaterials has been enormously exploited.[17–20] Venkatesan *et al.* have demonstrated the conjugation of gold nanoparticles with doxorubicin for improved cancer therapy.[21] Padhye *et al.* reported β-NaYF4:$Gd^{3+}$/$Tb^{3+}$ phosphor nanorods as anticancer drug delivery nanovehicles, targeting MCF-7 and NIH3T3 cells.[22] In

a recent study, the covalent immobilization of doxorubicin with glyhydroxyapatite nanoparticles was studied targeting WEHI-164 cells.[23] Furthermore, a polymeric multifaceted pH-responsive nanosystem with doxorubicin, targeting breast cancer by the proton sponge effect/endo-lysosomal escape system was reported.[24] In 2020, Mukherjee *et al.* described the rationale for designing PEGylated platinum nanoparticles using doxorubicin targeting melanoma under both *in vitro* and *in vivo* conditions.[25] To the best of our knowledge, studies pertaining to doxorubicin–PVP functionalized platinum nanoparticles targeting breast cancer are not reported so far.

In such circumstances, the present study uses poly-vinylpyrrolidone (PVP)-functionalized platinum nanoparticles having an octopod shape evidencing monodispersity. Further, platinum octopods were conjugated with doxorubicin for enhanced drug delivery and for minimizing the risk of drug toxicity. As a result, the doxorubicin–platinum conjugate system shows a substantial drug release profile and biocompatibility. Furthermore, the cytotoxic ability of the doxorubicin–platinum conjugate system was tested against two different intrinsic subtypes of breast cancer cells. Eventually, the molecular mechanism involved in the killing of breast cancer cell lines is revealed, substantiating the superior therapeutic potential of the doxorubicin–platinum conjugate system.

## 2. Materials and methods

### 2.1 Materials used

All the analytical chemicals used in the study were received from Sigma Aldrich, India. The cell culture-based chemicals are procured from Himedia Laboratories, India. The solvents used in the study were obtained from Sisco Research Laboratories, India. Antibodies used in the study were purchased from Cell Signalling Technologies (USA). All the purchased chemicals were used as received.

### 2.2 Synthesis of platinum octopods

In a typical synthesis, 35 mL of ethylene glycol (EG) was rapidly heated to 167 °C in the presence of sodium nitrate (NaNO$_3$) (0.163 g) and PVP ($M_w$: 10 000, 0.116 g).[26] After 5 min of the reaction, 5 mL of 10 mM chloroplatinic acid (H$_2$PtCl$_6$·2H$_2$O) was added, and the reaction was extended to 30 min until a black precipitate was obtained, thus concluding the formation of platinum nanoparticles. The product obtained was cooled to room temperature. Subsequently, the final product was obtained by centrifugation at 5000 rpm for 15 min at room temperature. The acquired pellet was then washed with a series of solvents such as acetone and hexane to remove unreacted products. The precipitate thus obtained is redispersed in 5 mL of ethanol and used further.

### 2.3 Conjugation reaction

For the conjugation reaction, 10 μg mL$^{-1}$ of doxorubicin was allowed to react with 50 μg mL$^{-1}$ of platinum octopods (2 mL) overnight under constant stirring.[21] After the reaction, the suspension was centrifuged at 12 000 rpm thrice to remove unreacted doxorubicin. In the end, the pellet is redispersed in 2 mL of Milli-Q water and stored for further use. The loading efficiency of doxorubicin on the surface of platinum octopods was measured using a spectrophotometer at 490 nm.

### 2.4 Characterization

UV-vis spectroscopy was performed to ascertain the formation of platinum octopods, conjugation reaction, and determine the loading efficiency of doxorubicin (Evolution-201, Thermo, USA). FT-IR measurements were performed to understand the involvement of functional groups during the formation of platinum octopods (Nicolet iS5, Thermo, USA). X-ray diffraction was performed to determine the presence of a face-centred cubic crystalline structure of platinum (X'Pert Pro PAnalytic, UK). The hydrodynamic diameter and zeta potential value of platinum octopods and the doxorubicin-conjugated theranostic system were determined *via* dynamic light scattering measurements (Zetasizer Nano-ZS90, Malvern, UK). High-resolution transmission electron microscopic studies were performed to ascertain the size and morphology of as-prepared platinum octopods (JEOL-2100+ high resolution transmission electron microscopy with SAED). The quenching effect between doxorubicin and platinum octopods was determined by a fluorescence spectrophotometer (Horiba Fluromax 4, USA).

### 2.5 *In vitro* drug release studies

The *in vitro* drug release studies were conducted to study the release behaviour of DOX from platinum octopods at two different pH values using phosphate buffer saline (pH 7.4) and acetate buffer (pH 4.5).[27] To achieve this, 2 mL of the doxorubicin–platinum conjugate system was sealed and placed in a dialysis bag ($M_w$: 12–14 kDa) with respective buffer systems (48 mL) at room temperature under constant stirring. At the pre-destined time, 2 mL of buffer from the system was removed and replaced with the same volume of the buffer with a similar pH. In the end, the release of doxorubicin from the platinum octopods was measured spectrophotometrically at 490 nm.

### 2.6 Cell culture experiments

The breast cancer cells (MCF-7 and MDA-MB-231) and normal human embryonic kidney (HEK-293) cells were procured from National Centre for Cell Science (NCCS), Pune, India. The cells were cultured in Dulbecco's Modified Eagle's Medium (DMEM) along with 10% fetal bovine serum (FBS) and 1% antibiotics (penicillin and streptomycin). The cells were maintained in an incubator with 5% CO$_2$ at 37 °C.

### 2.7 *In vitro* cytotoxicity and fluorescence-based staining

The *in vitro* cytotoxicity was assessed by the MTT (3-(4,5-dimethyl-thiazol-2-yl)-2,5-diphenyltetrazolium bromide) assay to determine the half-maximum inhibitory concentration (IC$_{50}$) of drugs such as doxorubicin, platinum octopods and platinum doxorubicin conjugates based on the methodology adopted by Mosmann *et al.*[28] Morphology-based fluorescence staining was executed to study live-dead, labelling nuclear DNA, generation

of reactive oxygen species, and mitochondrial membrane permeation studies according to the methodology reported earlier.[29] The cells were visualized and imaged under a fluorescence microscope (Accu-Scope, EXI-310, USA).

### 2.8 Semi-quantitative gene expression studies

RNA from $IC_{50}$ treated cells (with doxorubicin–platinum conjugate) and untreated cells were extracted and purified from breast cancer cells (MCF-7 and MDA-MB-231).[29] About 1 µg of total RNA was transcribed and amplified by PCR using specific primers to study cell survival and apoptosis-inducing genes (ESI Table 1†). The amplified PCR product was separated *via* electrophoresis, stained by ethidium bromide and visualized under the bioimaging system. In our study, β-actin served as an internal control.

### 2.9 Western blot analysis

The RIPA lysis buffer was used to separate proteins from $IC_{50}$ treated (doxorubicin–platinum conjugate) breast cancer cells, followed by quantification.[30] Later, proteins were separated by SDS-PAGE and electro-blotted onto a nitrocellulose membrane. Further, the membrane was blocked with nonfat milk for 1 h at 37 °C and probed further with primary antibodies (anti-p-Bcl-2; anti-p-caspase-9; anti-cleaved caspase-3; anti-cytochrome-c, anti-p-AKT, and anti-β-actin) overnight. Furthermore, TTBs buffer was used to wash the membrane, followed by incubating further with secondary antibodies for 1 h at 37 °C. In the end, the blots were developed using a chromogenic BCIP-NBT solution and recorded under a bioimaging system.

### 2.10 Statistical analysis

All the experiments performed in the study were expressed as mean ± SD. In addition, two-way ANOVA was performed. $P$-Value at $^{\#}P < 0.0001$, $^{***}P < 0.001$, $^{**}P < 0.01$, $^{*}P < 0.05$ and ns (non-significant) were considered statistically significant.

## 3. Result and discussion

In the present study, platinum nanoparticles using PVP ($M_w = 10\,000$) were synthesized by a polyol method, as shown in Scheme 1. The formation of PVP-functionalized platinum octopods was confirmed visually (yellow to black), followed by the UV-vis spectral analysis.[31] As shown in Fig. 1a, $PtCl_6^{2-}$ exhibits an absorbance peak at 212 and 268 nm. However, upon the start of the reaction, $PtCl_6^{2-}$ may undergo substitution, which results in the formation of nitroplatinate salt $(Pt(NO_2)_6^{2-})$ and leads to the disappearance of the peak at 268 nm. In our study, we inferred that the rate of nitroplatinate salt reduction into platinum nanoparticles is slow and time-dependent[26] (Fig. 1a). Taken together, this will be a key factor that results in the formation of anisotropic nanoparticles capped with PVP. The FT-IR spectrum confirmed the following vibration bands: –OH, C–H, C=O, $CH_2$ and C–N asymmetric stretching vibrations at 3364 cm$^{-1}$, 2975 cm$^{-1}$, 1656 cm$^{-1}$, 1383 cm$^{-1}$ and 1047 cm$^{-1}$, indicating the presence of PVP that functionalized the platinum nanoparticles (Fig. 1b). The XRD analysis confirmed the existence of a face-centred cubic crystalline structure of platinum coinciding well with earlier reported data with high purity and crystallinity (JCPDS: 004 0802)[32] (Fig. 1c). The hydrodynamic diameter of PVP-functionalized platinum octopods was found to be 173.5 ± 0.28 nm (Fig. 1d). In addition, zeta potential measurement suggests a negative surface charge value of −14.7 ± 8.16 mV (Fig. 1e). The negative zeta potential value is due to the capping of PVP on to the surface of platinum. According to the high resolution-transmission electron microscopy (HR-TEM) results, platinum nanoparticles showed an octopod shape with an average particle diameter between 10 and 19 nm (ref. [26 and 33]) (Fig. 2a–c). The SAED pattern shows the octopod-shaped platinum nanoparticle with the FCC structure crystal planes corresponding to {111}, {200}, {220}, and {311}, which is well in agreement with XRD results (Fig. 2d). Further, the as-prepared PVP functionalized platinum octopods were used for further conjugation experiments with a chemotherapeutic agent, doxorubicin.

As expected, the doxorubicin–platinum conjugate system developed was well dispersed in an aqueous medium, as shown in Scheme 2. In the present study, PVP used as a stabilizing agent for the preparation of platinum octopods acted as a linker with the $NH_2$ group of doxorubicin *via* electrostatic interaction/hydrogen bonding.[21,34] The interaction between doxorubicin and PVP-functionalized platinum octopods was confirmed by the UV-vis spectroscopic analysis with increased absorption (Fig. 3a). The loading efficiency of doxorubicin on the surface of PVP-functionalized platinum octopods was found to be ∼45%, as revealed by the Langmuir adsorption isotherm (Fig. 3b). We believe that interaction between PVP on the surface of platinum
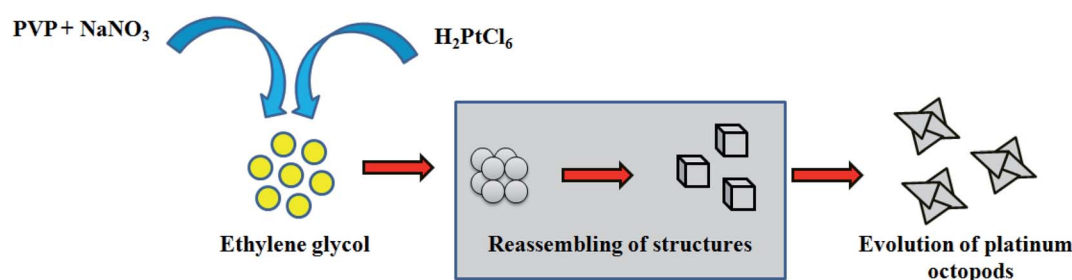


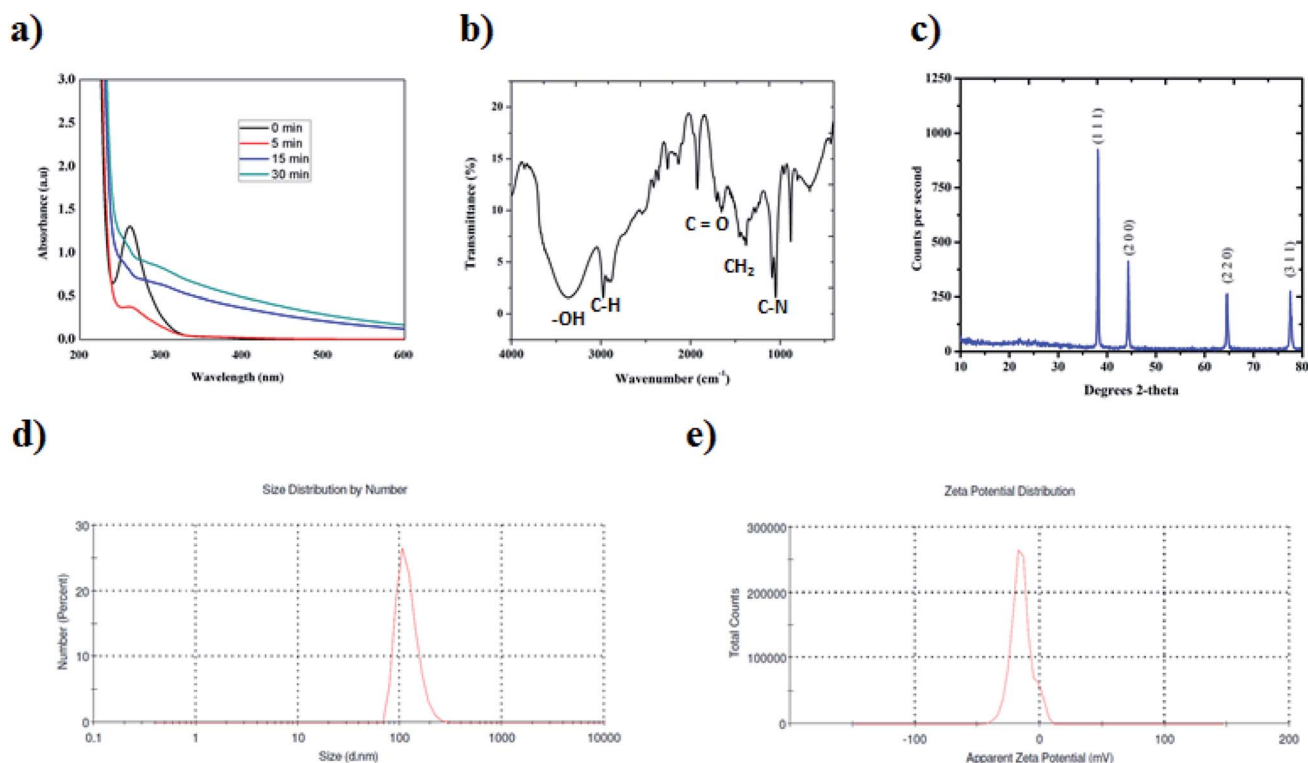**Scheme 1** Evolution of platinum octopods.

Fig. 1  High-throughput analytical characterization of platinum nanoparticles. (a) UV-vis spectroscopic studies at different time intervals. (b) FT-IR spectra analysis. (c) XRD analysis (the observed XRD plane matches JCPDS no. 004 0803).[32] (d) Particle size distribution analysis. (e) Zeta potential measurement studies.
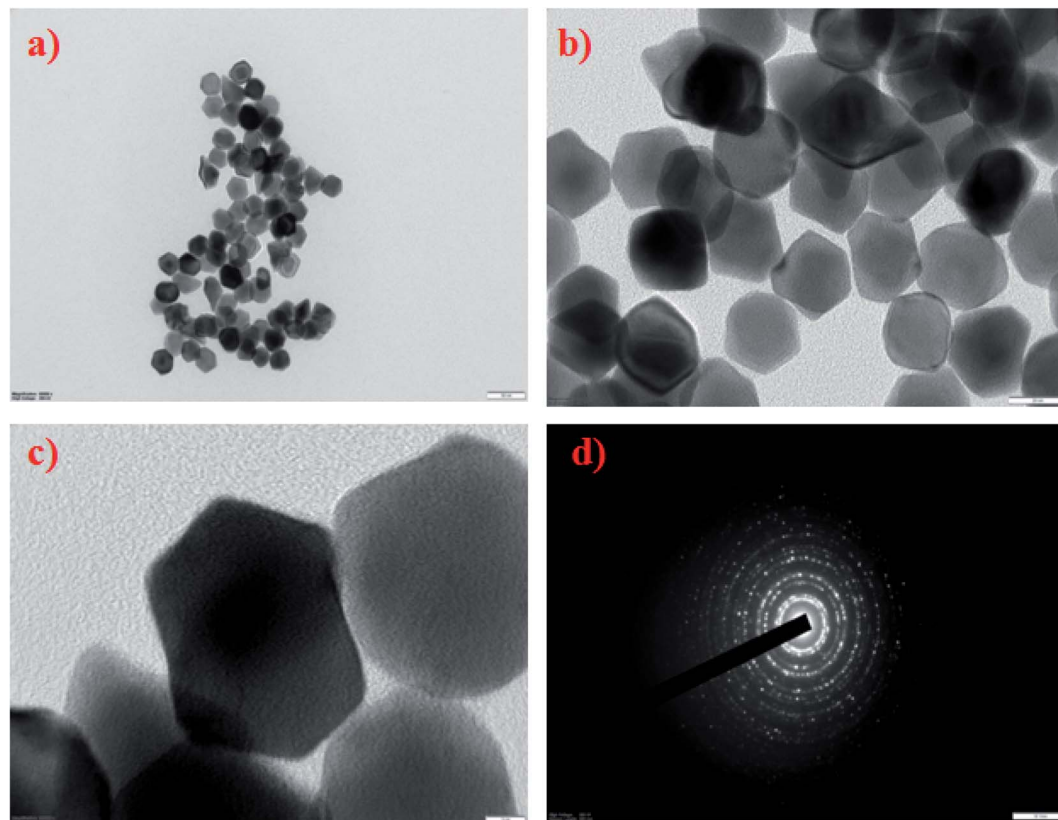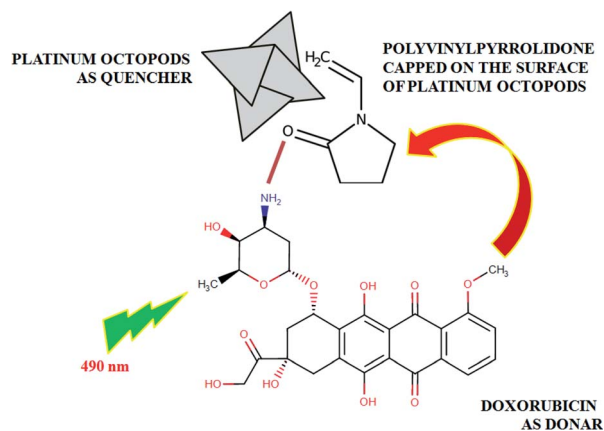


Fig. 2  High-resolution transmission electron microscopy studies of platinum octopods. (a and b) A view of octopod-shaped platinum nanoparticles. (c) A closure view at a 10 nm scale bar. (d) SAED pattern.

**Scheme 2** Quenching effect between platinum octopods (quencher) and doxorubicin (donor).

octopods drives the reaction between doxorubicin as a conjugate system (Scheme 1). As a result, the doxorubicin conjugated system showed an increased particle size distribution ($231 \pm 1.1$ nm) and a negative zeta potential ($-12.5 \pm 5.05$ mV) value (Fig. 3c and d). The results are consistent with earlier reports on the conjugation between gold nanorods and doxorubicin.[21]

Similarly, the fluorescence-based spectral analysis was used to verify the existence of doxorubicin onto the surface of platinum octopods by quenching studies. ESI Fig. 1a† shows that the quenching of doxorubicin on the metallic surface suggests the interaction of doxorubicin with PVP-functionalized platinum octopods at a shorter distance. The quenching is in good agreement with Stern–Volmer kinetics ($K_{sv} = 3.10 \times 10^4$ µg mL$^{-1}$), showing a strong relationship between the quencher and donor (ESI Fig. 1b†).

*In vitro* drug release studies of the doxorubicin–platinum conjugate system were carried out in phosphate buffer with pH 7.4 and in acetate buffer with pH 4.5 that replicates the pH mechanism of normal and cancerous cells, as shown in ESI Fig. 2.†[35] The relative release of doxorubicin from platinum nanoparticles is significantly higher in acetate buffer with pH 4.5 (43.2%), whereas only 25% of doxorubicin was released from the phosphate buffer with pH 7.4 for 48 h. We predict that the acidic pH breaks the electrostatic interaction/hydrogen bonding between doxorubicin and PVP-functionalized platinum octopods.[36] As a result, a sustained release of doxorubicin is achieved within the *in vitro* system and is time-dependent. However, this type of system should be carefully examined in normal cells to avoid non-specific side effects caused during conventional chemotherapy.
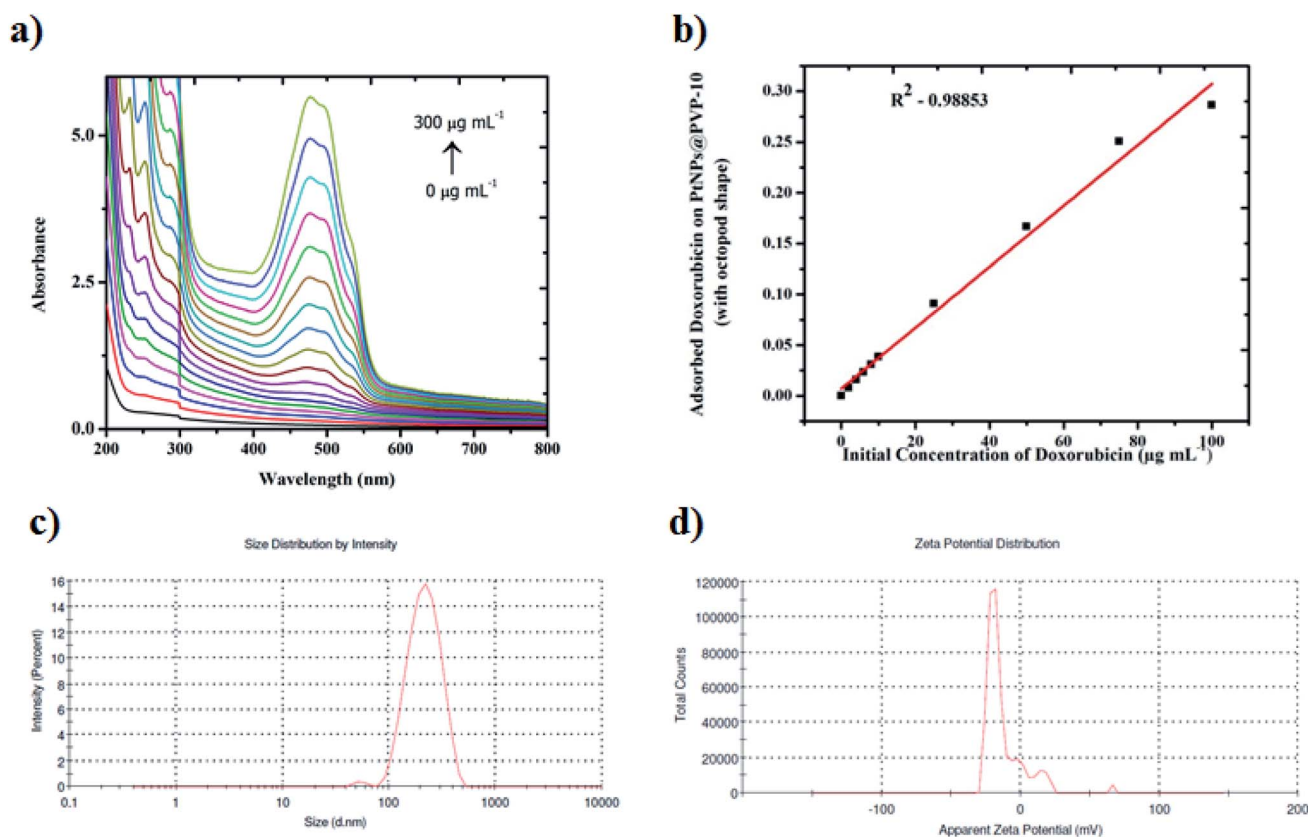


**Fig. 3** Conjugation of doxorubicin onto the surface of platinum octopods. (a) Development of extinction spectra upon the addition of different concentrations of doxorubicin (0–300 µg mL$^{-1}$) in the presence of platinum octopods. (b) Langmuir adsorption isotherm to determine the loading efficiency of doxorubicin onto the surface of platinum octopods. (c) Particle size distribution analysis. (d) Zeta potential measurement studies.
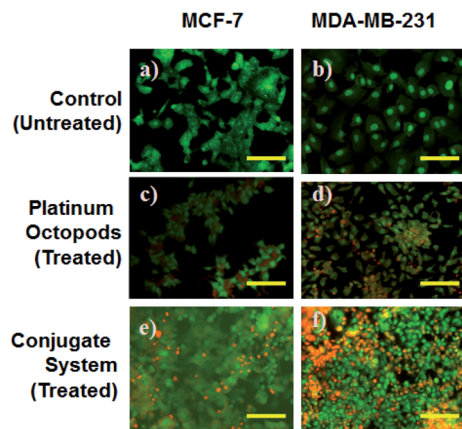
      

**Fig. 4** Dual staining by AO/EtBr for MCF-7 & MDA-MB-231 breast cancer cells with platinum octopods and doxorubicin–platinum conjugate system. (a and b) Control (untreated) cells. (c and d) Platinum octopod-treated cells. (e and f) Doxorubicin–platinum conjugate system-treated cells.



**Fig. 6** ROS studies by DCFH-DA for MCF-7 & MDA-MB-231 breast cancer cells with platinum octopods (PtNPs) and doxorubicin–platinum conjugate system. (a and b) Control (untreated) cells. (c and d) Platinum octopod-treated cells. (e and f) Doxorubicin–platinum conjugate system-treated cells.
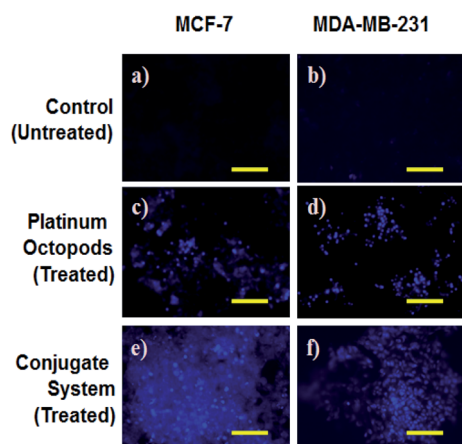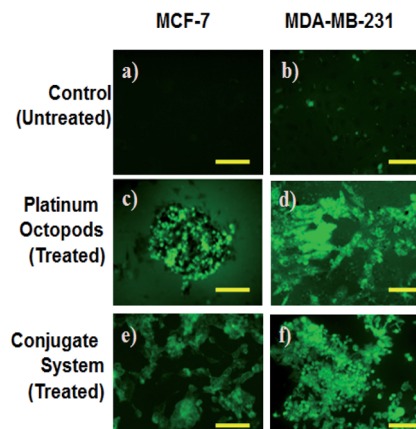


**Fig. 5** Nuclear staining by Hoechst 33444 for MCF-7 & MDA-MB-231 breast cancer cells with platinum octopods (PtNPs) and doxorubicin–platinum conjugate system. (a and b) Control (untreated) cells. (c and d) Platinum octopod-treated cells. (e and f) Doxorubicin–platinum conjugate system-treated cells.



**Fig. 7** Mitochondrial membrane potential studies by Rhodamine 123 for MCF-7 & MDA-MB-231 breast cancer cells with platinum octopods (PtNPs) and doxorubicin–platinum conjugate system. (a and b) Control (untreated) cells. (c and d) Platinum octopod-treated cells. (e and f) Doxorubicin–platinum conjugate system-treated cells.
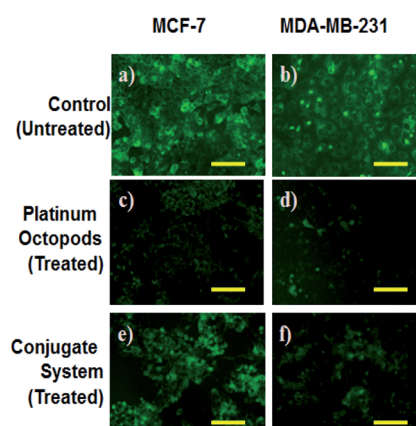
The MTT assay was performed to assess the anticancer effects of doxorubicin, platinum octopods and doxorubicin–platinum conjugate system with breast cancer cell lines (MCF-7 and MDA-MB-231).[37] Initially, free doxorubicin had increased toxicity compared to naked PVP-functionalized platinum octopods. However, a relatively high increased cytotoxicity value is noticed for the doxorubicin–platinum conjugate system due to the sustained release of doxorubicin from platinum octopods, as shown in ESI Table 2.† Also, a synergistic increase in efficacy upon conjugation between doxorubicin and PVP-functionalized platinum octopods is achieved.[21] The data from our study is consistent with *in vitro* release drug profile studies at different physiological pH values (4.5 and 7.4). However, the effect of the doxorubicin–platinum conjugate system was slightly higher in MCF-7 (2.099 ± 0.87 µg mL$^{-1}$) than that in MDA-MB-231 (3.196

± 0.51 µg mL$^{-1}$) cancer cells based on half-maximum inhibitory concentration. Moreover, the mechanism of killing cells by doxorubicin–platinum conjugate system is not known. Consequently, the doxorubicin–platinum conjugate system is not found to be toxic to HEK-293 (9.036 ± 0.73 µg mL$^{-1}$) cells compared to breast cancer cell lines (MCF-7 and MDA-MB-231). Based on the data, the doxorubicin–platinum conjugate system kills breast cancer cells more efficiently than normal cells. In all cases, no signs of cell death were observed in control, *i.e.*, untreated cells.

A fluorescence microscope was employed to study the induction of apoptosis by a doxorubicin–platinum conjugate system against breast cancer (MCF-7 and MDA-MB-231) cells.[37] Fig. 4–7 show the ability of platinum octopods and doxorubicin–platinum conjugate system in inducing apoptosis, nuclear beading, reactive oxygen species (ROS), and
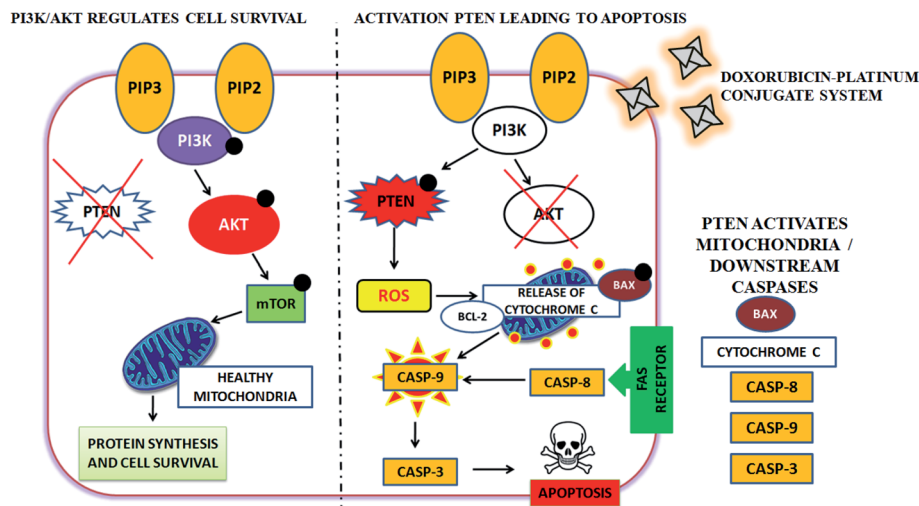
**Scheme 3** Targeting PI3K/AKT pathway by upregulating PTEN on treatment with doxorubicin–platinum conjugate system.
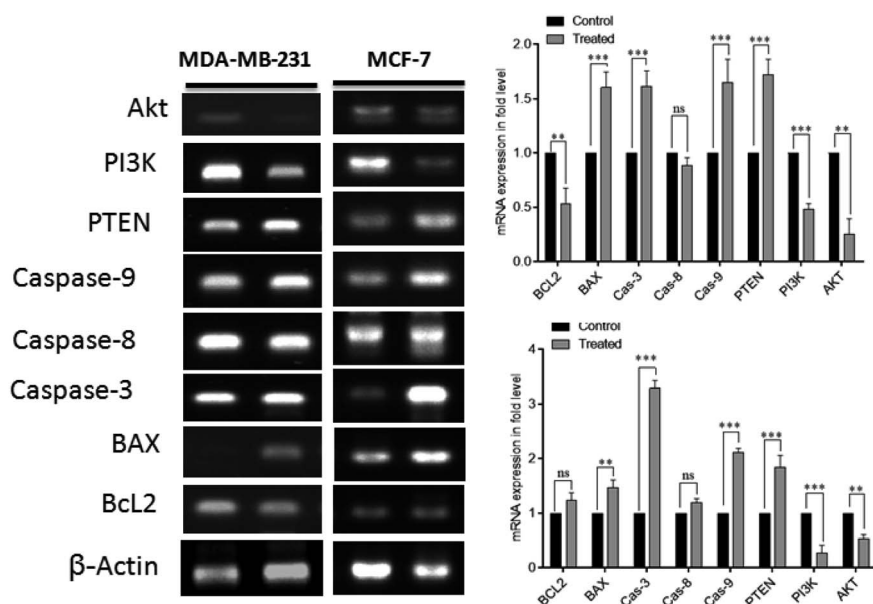


**Fig. 8** Semi-quantitative RT-PCR gene expression studies of the doxorubicin–platinum conjugate system against breast cancer cells (MCF-7 and MDA-MB-231). Representative blots of at least three separate experiments are shown (left-hand panel). Quantification of genes and proteins were performed for (a) and (b) (right-hand panel).

mitochondrial membrane potential in breast cancer (MCF-7 and MDA-MB-231) cells. At first, dual staining involving acridine orange (AO) and ethidium bromide (EtBr) was performed to determine the cellular apoptosis, as shown in Fig. 4. Upon exposure to $IC_{50}$ concentration, the cells under the fluorescence microscope display the apoptotic morphology with cells stained in red due to chromatin condensation, nuclear beading, and fragmentation. Moreover, the normal cells appear to be green, evidencing that apoptosis did not occur. Secondly, the evidence of the formation of pyknotic nuclei upon treatment with the doxorubicin-conjugate system was evaluated by nuclear staining involving Hoechst 33444 dye. Upon treatment, the cells showed a change in the nuclear morphology, inferring the pyknotic nucleus with blue emission.

In the same way, no blue emission is noticed in the control cells (Fig. 5). Thirdly, the generation of ROS upon treatment with the doxorubicin–platinum conjugate system is studied with the DCFH-DA dye. DCFH-DA upon entry into cells interacts with free radicals and gets converted into a fluorogenic compound called DCF with green emission. In our study, the doxorubicin-conjugate system induces the generation of ROS with green emission under a fluorescence microscope (Fig. 6). The increase in the fluorescence intensity by ROS generation with reference to control cells is plotted, as shown in ESI Fig. 3.† At last, the induction of the mitochondrial membrane potential
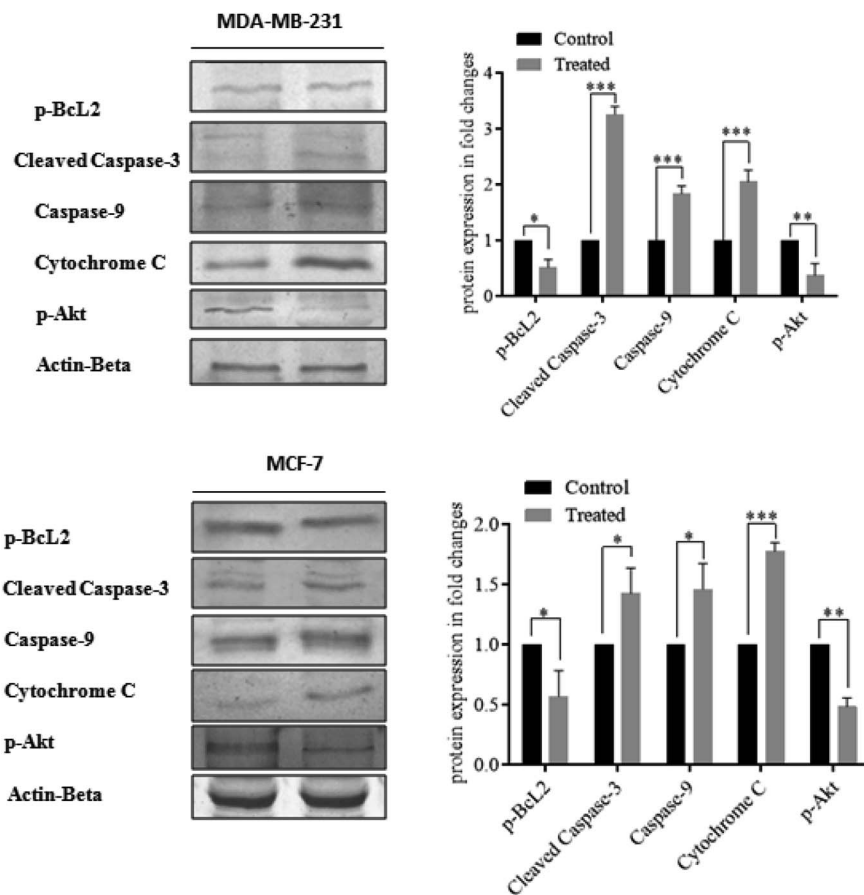
**Fig. 9** Western blotting studies of doxorubicin–platinum conjugate system against breast cancer cells (MCF-7 and MDA-MB-231). Representative blots of at least three separate experiments are shown (left-hand panel). Quantification of genes and proteins were performed for (a) and (b) (right-hand panel).

in breast cancer cells is visualized using Rhodamine 123, as shown in control (Fig. 7). Rhodamine 123 explicitly stains mitochondria green, with a distinct structure. However, in the case of the doxorubicin–platinum conjugate system, a disoriented structure is observed, indicating the damage of cells is noticed (Fig. 7d and f). In all cases, the control cells show no significant morphological changes, as shown in Fig. 4–7(a). From the obtained results, we predict that doxorubicin upon conjugation triggers increased apoptosis due to the sustained release of doxorubicin than naked PVP-functionalized platinum octopods. Hence, the results of cytotoxicity and fluorescence microscopy were consistent with the support of the doxorubicin–platinum conjugate system, targeting breast cancer cells as a model.[21] However, molecular mechanisms are deliberately needed to substantiate the above-mentioned results.

Moreover, cellular pathways that promote apoptosis are the clinically binding targets of anticancer drugs.[38–41] From this perspective, we examined the effects of the doxorubicin–platinum conjugate system on targeted cellular pathways to induce apoptosis, as shown in Scheme 3. The PI3K/AKT pathway is essential for critical cellular functions such as cell growth, proliferation, motility, survival, and angiogenesis.[42] Several studies demonstrated that the aberrant activation of PI3K/AKT

pathways leads to the resistance of apoptosis in cancer cells.[43] However, the PI3K/AKT signalling pathway is counteracted by phosphatase and tensin homolog (PTEN), which inhibits the PI3K/AKT-mediated activation of downstream kinases.[44,45] Therefore, we have analyzed the expression profile by RT-PCR (PI3K, AKT, and PTEN) and western blot (AKT) analysis (Fig. 8 and 9). We observed that the doxorubicin–platinum conjugate-treated breast cancer cells showed a down-regulated mRNA expression of PI3K and AKT (Fig. 8). The western blot analysis further confirmed the decreased expression of AKT (Fig. 9). On the contrary, the relative mRNA expression of PTEN was significantly increased in breast cancer cells treated with the doxorubicin–platinum conjugate (Fig. 8). Therefore, PTEN exerts tumour-suppressive effect and may induce apoptosis by attenuating PI3K/AKT signalling *via* the dephosphorylating of PIP3 to PIP2.[46,47]

Besides, it has been reported that mitochondria are the crucial target for the intrinsic apoptotic pathway by releasing cytochrome c that massively activates the downstream caspases, triggering cell death.[48] Consequently, we have examined the transcriptional regulation of genes involved in the mitochondrion-mediated apoptosis[49] (Fig. 8 and 9). The BCL-2 gene involved in controlling the permeabilization of

mitochondrial outer membranes was found to be significantly down-regulated in doxorubicin–platinum conjugate-treated cancer cells.[50] Moreover, the relative mRNA expression of pro-apoptotic genes such as BAX and cytochrome c is highly upregulated[51] (Fig. 8 and 9). The mitochondrial membrane depolarization allows the release of cytochrome c and thus results in the irreversible activation of caspases and cell death. On that premise, the breast cancer cells treated with the doxorubicin–platinum conjugate showed increased upregulation of caspases 3 and 9 (Fig. 8 and 9). The released cytochrome c binds to the apoptotic protease activating factor 1 (APAF-1), promotes the oligomerization and activation of caspase 9 at the apoptosome complex, which in turn leads to the activation of caspase 3 (Fig. 8 and 9). The activated caspase 3 drives cell proteolysis that entails chromatin condensation, DNA breakage, and cell annihilation and coexists with fluorescence microscopic studies.[52] Besides, our study also revealed that the elevated expressions of caspase 8 have an essential role in the extrinsic apoptosis pathway in MCF-7 breast cancer cell lines (Fig. 8). Caspase 8 binds with adaptor protein FADD (a member of death domain superfamily) to form a death-inducing signalling complex (DISC) and subsequently initiates the downstream cleavage of caspase 3 *via* mitochondrial-dependent pathways[53] (Fig. 9). However, no such upregulation is noticed in MDA-MB-231 breast cancer cell lines (Fig. 8). Taken in conjunction, our findings suggest that the treatment of the doxorubicin–platinum conjugate in breast cancer cells potentially induced mitochondrial-dependent apoptosis through the activation of the tumour suppressor gene (PTEN) and the downregulation of the anti-apoptotic gene BCL-2 *via* mitochondrial dysfunction.

## 4. Conclusion

In this study, we have established the formulation and characterization of the doxorubicin–platinum conjugate system. The obtained doxorubicin–platinum conjugate system acquired anticancer activity against breast cancer cells (MCF-7 and MDA-MB-231) by limiting the PI3K/AKT signalling pathway *via* the activation of the tumour suppressor gene, *PTEN*. Ultimately, this led to mitochondrial dysfunction and actuation of downstream caspases for apoptotic cell death in cancer cells. Therefore, the stability, persistent drug release and anticancer efficacy of a developed doxorubicin–platinum conjugate system would have a potential role in biomedical applications, including cancer treatment and drug delivery.

## Conflicts of interest

There are no conflicts to declare.

## Acknowledgements

## References

1 S. Baek, *et al.*, Smart multifunctional drug delivery towards anticancer therapy harmonized in mesoporous nanoparticles, *Nanoscale*, 2015, **7**, 14191–14216.

2 A. Kumari, *et al.*, Isolation, Characterization and In Silico Study of Conotoxin Protein from Conus loroisii and Its Anti-cancer Activity, *Int. J. Pept. Res. Ther.*, 2020, DOI: 10.1007/s10989-020-10091-x.

3 J. Kydd, *et al.*, Targeting Strategies for the Combination Treatment of Cancer Using Drug Delivery Systems, *Pharmaceutics*, 2017, **9**, 46.

4 A. Khoury, K. M. Deo and J. R. Aldrich-Wright, Recent advances in platinum-based chemotherapeutics that exhibit inhibitory and targeted mechanisms of action, *J. Inorg. Biochem.*, 2020, **207**, 111070.

5 S. Dilruba and G. V. Kalayda, Platinum-based drugs: past, present and future, *Cancer Chemother. Pharmacol.*, 2016, **77**, 1103–1124.

6 L. Kelland, The resurgence of platinum-based cancer chemotherapy, *Nat. Rev. Cancer*, 2007, **7**, 573–584.

7 X.-J. Liang, C. Chen, Y. Zhao and P. C. Wang, Circumventing Tumor Resistance to Chemotherapy by Nanotechnology, in *Multi-Drug Resistance in Cancer*, ed. J. Zhou, Humana Press, 2010, vol. 596, pp. 467–488.

8 G. Housman, *et al.*, Drug Resistance in Cancer: An Overview, *Cancers*, 2014, **6**, 1769–1792.

9 J. K. Patra, *et al.*, Nano based drug delivery systems: recent developments and future prospects, *J. Nanobiotechnol.*, 2018, **16**, 71.

10 K. M. Koczkur, S. Mourdikoudis, L. Polavarapu and S. E. Skrabalak, Polyvinylpyrrolidone (PVP) in nanoparticle synthesis, *Dalton Trans.*, 2015, **44**, 17883–17905.

11 F. Gal, *et al.*, Electrocatalytic (Bio)Nanostructures Based on Polymer-Grafted Platinum Nanoparticles for Analytical Purpose, *ACS Appl. Mater. Interfaces*, 2016, **8**, 14747–14755.

12 J. Xu, Y. Hu, S. Wang, X. Ma and J. Guo, Nanomaterials in electrochemical cytosensors, *Analyst*, 2020, **145**, 2058–2069.

13 V. A. Volochaev, I. N. Novomlinskii, E. M. Bayan and V. E. Guterman, Nanostructured Platinum Catalyst Supported by Titanium Dioxide, *Russ. J. Electrochem.*, 2019, **55**, 1021–1030.

14 I. Khan, K. Saeed and I. Khan, Nanoparticles: properties, applications and toxicities, *Arabian J. Chem.*, 2019, **12**, 908–931.

15 J. V. McGowan, *et al.*, Anthracycline Chemotherapy and Cardiotoxicity, *Cardiovasc. Drugs Ther.*, 2017, **31**, 63–75.

16 G. N. Hortobágyi, Anthrazykline in der Krebstherapie: Ein Überblick, *Drugs*, 1997, **54**, 1–7.

17 K. R. Javed, *et al.*, Comparison of Doxorubicin Anticancer Drug Loading on Different Metal Oxide Nanoparticles, *Medicine*, 2015, **94**, e617.

18 K. Ulbrich, *et al.*, Targeted Drug Delivery with Polymers and Magnetic Nanoparticles: Covalent and Noncovalent Approaches, Release Control, and Clinical Studies, *Chem. Rev.*, 2016, **116**, 5338–5431.

19 S. K. Sahoo and V. Labhasetwar, Enhanced Antiproliferative Activity of Transferrin-Conjugated Paclitaxel-Loaded Nanoparticles is Mediated via Sustained Intracellular Drug Retention, *Mol. Pharmaceutics*, 2005, **2**, 373–383.

20 P. N. Navya, *et al.*, Current trends and challenges in cancer management and therapy using designer nanomaterials, *Nano Convergence*, 2019, **6**, 23.

21 R. Venkatesan, *et al.*, Doxorubicin conjugated gold nanorods: a sustained drug delivery carrier for improved anticancer therapy, *J. Mater. Chem. B*, 2013, **1**, 1010–1018.

22 P. Padhye, A. Alam, S. Ghorai, S. Chattopadhyay and P. Poddar, Doxorubicin-conjugated β-NaYF$_4$:Gd$^{3+}$/Tb$^{3+}$ multifunctional, phosphor nanorods: a multi-modal, luminescent, magnetic probe for simultaneous optical and magnetic resonance imaging and an excellent pH-triggered anti-cancer drug delivery nanovehicle, *Nanoscale*, 2015, **7**, 19501–19518.

23 G. Verma, *et al.*, Covalent immobilization of doxorubicin in glycine functionalized hydroxyapatite nanoparticles for pH-responsive release, *New J. Chem.*, 2018, **42**, 6283–6292.

24 S. V. Lale, A. Kumar, F. Naz, A. C. Bharti and V. Koul, Multifunctional ATRP based pH responsive polymeric nanoparticles for improved doxorubicin chemotherapy in breast cancer by proton sponge effect/endo-lysosomal escape, *Polym. Chem.*, 2015, **6**, 2115–2132.

25 S. Mukherjee, *et al.*, Improved delivery of doxorubicin using rationally designed PEGylated platinum nanoparticles for the treatment of melanoma, *Mater. Sci. Eng., C*, 2020, **108**, 110375.

26 T. Herricks, J. Chen and Y. Xia, Polyol Synthesis of Platinum Nanoparticles: Control of Morphology with Sodium Nitrate, *Nano Lett.*, 2004, **4**, 2367–2371.

27 E. Ahnfelt, E. Sjögren, P. Hansson and H. Lennernäs, In Vitro Release Mechanisms of Doxorubicin From a Clinical Bead Drug-Delivery System, *J. Pharm. Sci.*, 2016, **105**, 3387–3398.

28 T. Mosmann, Rapid colorimetric assay for cellular growth and survival: application to proliferation and cytotoxicity assays, *J. Immunol. Methods*, 1983, **65**, 55–63.

29 P. Kumar, S. Senthamilselvi, M. Govindaraju and R. Sankar, Unraveling the caspase-mediated mechanism for phloroglucinol-encapsulated starch biopolymer against the breast cancer cell line MDA-MB-231, *RSC Adv.*, 2014, **4**, 46157–46163.

30 P. Kumar, M. Kannan, V. ArunPrasanna, B. Vaseeharan and S. Vijayakumar, Proteomics analysis of crude squid ink isolated from Sepia esculenta for their antimicrobial, antibiofilm and cytotoxic properties, *Microb. Pathog.*, 2018, **116**, 345–350.

31 M. I. Mendivil Palma, *et al.*, Synthesis and Properties of Platinum Nanoparticles by Pulsed Laser Ablation in Liquid, *J. Nanomater.*, 2016, **2016**, e9651637, https://www.hindawi.com/journals/jnm/2016/9651637/.

32 I. A. Safo, M. Werheid, C. Dosche and M. Oezaslan, The role of polyvinylpyrrolidone (PVP) as a capping and structure-directing agent in the formation of Pt nanocubes, *Nanoscale Adv.*, 2019, **1**, 3095–3106.

33 L. Dai, *et al.*, Controlled synthesis of novel octapod platinum nanocrystals under microwave irradiation, *Mater. Res. Bull.*, 2014, **49**, 413–419.

34 A. Rudra, R. M. Deepa, M. K. Ghosh, S. Ghosh and B. Mukherjee, Doxorubicin-loaded phosphatidylethanolamine-conjugated nanoliposomes: in vitro characterization and their accumulation in liver, kidneys, and lungs in rats, *Int. J. Nanomed.*, 2010, **5**, 811–823.

35 S. Parveen, R. Misra and S. K. Sahoo, Nanoparticles: a boon to drug delivery, therapeutics, diagnostics and imaging, *Nanomedicine*, 2012, **8**, 147–166.

36 B. Subia, S. Chandra, S. Talukdar and S. C. Kundu, Folate conjugated silk fibroin nanocarriers for targeted drug delivery, *Integr. Biol.*, 2014, **6**, 203–214.

37 P. Kumar, S. Senthamilselvi and M. Govindaraju, Phloroglucinol-encapsulated starch biopolymer: preparation, antioxidant and cytotoxic effects on HepG2 liver cancer cell lines, *RSC Adv.*, 2014, **4**, 26787.

38 G. Pistritto, D. Trisciuoglio, C. Ceci, A. Garufi and G. D'Orazi, Apoptosis as anticancer mechanism: function and dysfunction of its modulators and targeted therapeutic strategies, *Aging*, 2016, **8**, 603–619.

39 W. An, *et al.*, Apoptotic Pathway as the Therapeutic Target for Anticancer Traditional Chinese Medicines, *Front. Pharmacol.*, 2019, **10**, 758.

40 I. R. Indran, G. Tufo, S. Pervaiz and C. Brenner, Recent advances in apoptosis, mitochondria and drug resistance in cancer cells, *Biochim. Biophys. Acta, Bioenerg.*, 2011, **1807**, 735–745.

41 J. S. Long and K. M. Ryan, New frontiers in promoting tumour cell death: targeting apoptosis, necroptosis and autophagy, *Oncogene*, 2012, **31**, 5045–5060.

42 N. Sadeghi and D. E. Gerber, Targeting the PI3K pathway for cancer therapy, *Future Med. Chem.*, 2012, **4**, 1153–1169.

43 W. J. Davis, P. Z. Lehmann and W. Li, Nuclear PI3K signaling in cell growth and tumorigenesis, *Front. Cell Dev. Biol.*, 2015, **3**, 24.

44 N. Chalhoub and S. J. Baker, PTEN and the PI3-Kinase Pathway in Cancer, *Annu. Rev. Pathol.: Mech. Dis.*, 2009, **4**, 127–150.

45 M.-M. Georgescu, PTEN Tumor Suppressor Network in PI3K-Akt Pathway Control, *Genes Cancer*, 2010, **1**, 1170–1177.

46 I. Pal and M. Mandal, PI3K and Akt as molecular targets for cancer therapy: current clinical outcomes, *Acta Pharmacol. Sin.*, 2012, **33**, 1441–1458.

47 A. Carnero and J. M. Paramio, The PTEN/PI3K/AKT Pathway in vivo, Cancer Mouse Models, *Front. Oncol.*, 2014, **4**(252), 1–10.

48 A. Shamas-Din, J. Kale, B. Leber and D. W. Andrews, Mechanisms of Action of Bcl-2 Family Proteins, *Cold Spring Harbor Perspect. Biol.*, 2013, **5**(4), DOI: 10.1101/cshperspect.a008714.
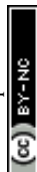
49 M. H. Naseri, *et al.*, Up regulation of Bax and down regulation of Bcl2 during 3-NC mediated apoptosis in human cancer cells, *Cancer Cell Int.*, 2015, **15**, 55.

50 E. Gottlieb, S. M. Armour, M. H. Harris and C. B. Thompson, Mitochondrial membrane potential regulates matrix configuration and cytochrome c release during apoptosis, *Cell Death Differ.*, 2003, **10**, 709–717.

51 X. Jiang and X. Wang, Cytochrome c Promotes Caspase-9 Activation by Inducing Nucleotide Binding to Apaf-1, *J. Biol. Chem.*, 2000, **275**, 31199–31203.

52 A. G. Porter and R. U. Jänicke, Emerging roles of caspase-3 in apoptosis, *Cell Death Differ.*, 1999, **6**, 99–104.

53 B. Tummers and D. R. Green, Caspase-8; regulating life and death, *Immunol. Rev.*, 2017, **277**, 76–89.